

# Complete Next-to-Leading Order QCD Corrections to $ZZ$ Production in Gluon Fusion


Bakul Agarwal<sup>1,2,\*</sup>, Stephen Jones<sup>3,†</sup>, Matthias Kerner<sup>1,‡</sup> and Andreas von Manteuffel<sup>4,2,§</sup>

<sup>1</sup>*Institute for Theoretical Physics, Karlsruhe Institute of Technology (KIT), D-76131 Karlsruhe, Germany*

<sup>2</sup>*Department of Physics and Astronomy, Michigan State University, East Lansing, Michigan 48824, USA*

<sup>3</sup>*Institute for Particle Physics Phenomenology, Durham University, Durham DH1 3LE, United Kingdom*

<sup>4</sup>*Institut für Theoretische Physik, Universität Regensburg, 93040 Regensburg, Germany*

 (Received 20 April 2024; revised 18 October 2024; accepted 20 December 2024; published 22 January 2025)

We calculate the complete next-to-leading order (NLO) QCD corrections to loop-induced  $gg \rightarrow ZZ$  production including full top-quark mass effects. The two-loop virtual corrections are obtained by combining analytic results for the massless, Higgs-mediated, and one-loop factorizable contributions with numerically computed amplitudes containing the top-quark mass. We show that the choice of subtraction scheme for the virtual contribution impacts the precision with which the virtual contribution must be evaluated in order to obtain sufficiently precise phenomenological predictions. For direct production through a massive top-quark loop, we observe that the relative NLO corrections are large. The direct massive and Higgs-mediated contributions individually increase relative to the massless production at high diboson invariant mass, but interfere destructively with each other. At the Large Hadron Collider, the NLO corrections to the gluon channel give a sizable contribution to the  $pp \rightarrow ZZ + X$  cross section at  $N^3\text{LO}$ .

DOI: [10.1103/PhysRevLett.134.031901](https://doi.org/10.1103/PhysRevLett.134.031901)

**Introduction**—The advent of the High-Luminosity LHC brings exciting opportunities to measure standard model parameters at unprecedented precision. An important process in this regard is  $Z$  pair production, which is relevant for new physics searches [1–4] and provides a significant background to Higgs production in the four-lepton channel [5–8], both for on- and off-shell Higgs bosons.  $Z$  boson pair production has been measured at 13.6 TeV [9] and used to constrain anomalous  $CP$ -odd neutral triple gauge couplings [10]. Comparing resonant and nonresonant Higgs production allows for an indirect probe of the Higgs width [11,12], and continuum  $Z$  pair production can contribute significantly to off-shell Higgs production through interference [13,14]. Constraints on the Higgs width have been obtained in this way by CMS [15] and ATLAS experiments [16]. Given the phenomenological relevance, precise theoretical predictions for this process are desirable.

The gluon fusion channel for  $Z$  pair production is loop-induced and starts to contribute to the hadronic process  $pp \rightarrow ZZ + X$  only at next-to-next-to-leading order (NNLO).

Owing to high gluon luminosity at the LHC, this channel accounts for  $O(60\%)$  of the total NNLO correction [17]. NLO corrections to this channel are formally next-to-next-to-next-to-leading order with respect to the hadronic process. In general, different partonic channels mix at higher orders in the perturbative expansion such that the concept of corrections to a specific subprocess is not well defined. In the present case, however, one can define NLO corrections to the gluon channel by considering only the contributions in which neither of the  $Z$  bosons couples to external quark lines. The so-defined NLO corrections are indeed significant; estimates [18,19] give an overall  $O(5\text{--}8\%)$  increase to the total  $pp \rightarrow ZZ$  cross section.

For the two-loop amplitudes, the massless corrections were computed a while back in [20,21], while the top-quark contributions remained a challenge until recently, preventing the calculation of the exact NLO QCD corrections in this channel so far. The top-quark contributions are expected to be important, particularly in the high invariant mass region for the production of longitudinal  $Z$  bosons due to the Goldstone boson equivalence theorem [22,23] and the interplay with Higgs-mediated production. Approximate NLO corrections to  $gg \rightarrow ZZ$  have been presented in [24–28] and supplemented with a parton shower in [29,30]. Recently, the two-loop amplitudes have been calculated with full top-quark mass effects [31,32].

In this Letter, we take the next step and calculate the complete NLO QCD corrections to  $gg \rightarrow ZZ$  with full top-quark mass effects. Specifically, we consider all contributions to the cross section involving closed massless or massive quark loops to which the external  $Z$  bosons couple

\*Contact author: bakul.agarwal@kit.edu

†Contact author: stephen.jones@durham.ac.uk

‡Contact author: matthias.kerner@kit.edu

§Contact author: manteuffel@ur.de

Published by the American Physical Society under the terms of the [Creative Commons Attribution 4.0 International license](https://creativecommons.org/licenses/by/4.0/). Further distribution of this work must maintain attribution to the author(s) and the published article's title, journal citation, and DOI. Funded by SCOAP<sup>3</sup>.

either directly or through a Higgs boson. For the real radiation contributions, we take into account also  $gq$ ,  $g\bar{q}$ , and  $q\bar{q}$  in addition to  $gg$  initial states. Using a fully differential setup, we compute the inclusive cross section and the diboson invariant mass distribution for  $ZZ$  production at the LHC.

*Details of the calculation*—The differential cross section for  $gg \rightarrow ZZ$  at NLO can be written as  $d\sigma_{\text{NLO}} = d\sigma_{\text{B}} + d\sigma_{\text{V}} + d\sigma_{\text{R}}$ , where  $d\sigma_{\text{B}}$ ,  $d\sigma_{\text{V}}$ , and  $d\sigma_{\text{R}}$  correspond to Born, virtual, and real contributions, respectively. In our calculation, we include effects due to  $n_f = 5$  massless quark flavors, a massive top quark, and a massive Higgs boson. The calculation of the different contributions is described below.

**Born and virtual contributions:** We consider the partonic process

$$g(p_1) + g(p_2) \longrightarrow Z(p_3) + Z(p_4), \quad (1)$$

for on-shell momenta, i.e.,  $p_1^2 = p_2^2 = 0$  and  $p_3^2 = p_4^2 = m_Z^2$ .

The one-loop amplitudes relevant for the Born contribution were calculated long ago in Refs. [33–35], while the two-loop corrections employed for this Letter were completed only recently. We distinguish between different classes of contributions to the amplitude, depending on the couplings of the external  $Z$  bosons. Figure 1 shows a representative two-loop Feynman diagram for each of the following classes.

*Class  $A_h$ :* Both  $Z$  bosons couple directly to the same heavy top-quark loop. For these one- and two-loop contributions, we use the recent calculation [31] by some of us that employed a combination of syzygy techniques [31,36–40], finite field methods [41,42], multivariate partial fractioning [43–47], and constructions of finite integrals, and the resulting finite master integrals were evaluated numerically with pySecDec [48–50].

*Class  $A_l$ :* Both  $Z$  bosons couple directly to the same light quark loop. Analytical expressions for these one- and two-loop contributions were provided in [20], based on solutions for the master integrals [51] in terms of multiple polylogarithms. We employ their implementation in the vVamp library and numerically evaluate the multiple polylogarithms using the code of [52] included in GiNaC [53].

*Class B:* The  $Z$  bosons couple to different closed quark loops, each of which can be a light or a heavy quark. At two loops, these corrections are one-particle reducible products of one-loop triangles. These are the only diagrams involving Dirac traces with an odd number of  $\gamma_5$  matrices and contributions related to the chiral anomaly can arise due to a mass splitting within a weak isodoublet. Consequently, one should consider them for sums over a complete quark generation, and for our calculation with five massless quarks just the third generation contributes due to  $m_b \neq m_t$ . These contributions have been presented in [26]; we use the recalculation in [31] for this work.

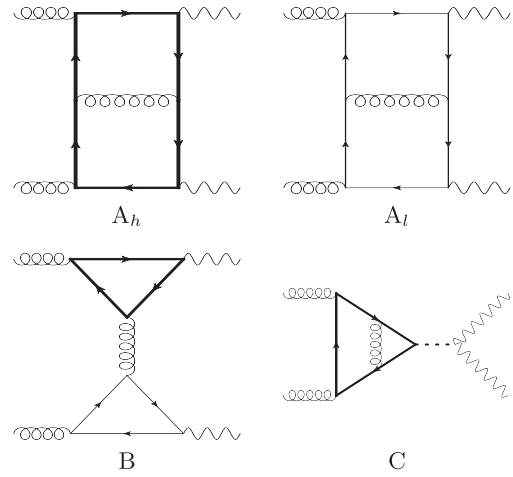


FIG. 1. Representative two-loop diagrams with closed quark loops entering the virtual corrections to  $ZZ$  production. Thick lines denote top quarks.

*Class C:* The  $Z$ -boson pair is produced via the decay of an intermediate off-shell Higgs boson, which couples to a heavy quark loop. We employ an in-house implementation of these Higgs-mediated contributions based on the differential equations approach, similar to the calculation in [54]. In the high invariant mass region, above the top-quark threshold, one finds interesting interferences between the Higgs-mediated and direct production of longitudinally polarized  $Z$  bosons. At one loop, it has been discussed in [34] that the interference is destructive and exhibits a cancellation of the leading term at high energy, as required by the unitarity of the  $t\bar{t} \rightarrow ZZ$  subprocess; we observe a strong destructive interference also at two loops.

After UV renormalization and IR subtraction, details of which are provided in Refs. [20,31], the finite remainders for the helicity amplitudes can be written as

$$\mathcal{M}_\lambda^{\text{fin}} = \left(\frac{\alpha_s}{2\pi}\right) \mathcal{M}_\lambda^{(1)} + \left(\frac{\alpha_s}{2\pi}\right)^2 \mathcal{M}_\lambda^{(2)} + \mathcal{O}(\alpha_s^3), \quad (2)$$

where  $\lambda = \{\lambda_1, \lambda_2, \lambda_3, \lambda_4\}$  specify the polarizations of the external particles. Here,  $\mathcal{M}_\lambda^{(1)}$ ,  $\mathcal{M}_\lambda^{(2)}$  are the one- and two-loop finite remainders constructed from the form factor decomposition described in [20].

We define the squared one-loop amplitude  $\mathcal{V}^{(1)}$  as

$$\mathcal{V}^{(1)} = \frac{1}{N} \sum_{\lambda, \text{color}} \mathcal{M}_\lambda^{*(1)} \mathcal{M}_\lambda^{(1)}, \quad (3)$$

where we divide by  $N = 2^2 \times 8^2 \times 2$  to account for the averaging over spins and colors in the initial state and the symmetry factor due to identical particles in the final state. To optimize the sampling of the two-loop amplitude for our full result, we separate it according to the classes defined above,

$$\mathcal{M}_\lambda^{(2)} = \mathcal{M}_{\lambda,A_h}^{(2)} + \mathcal{M}_{\lambda,A_t}^{(2)} + \mathcal{M}_{\lambda,B}^{(2)} + \mathcal{M}_{\lambda,C}^{(2)}. \quad (4)$$

The interference with the full Born amplitude  $\mathcal{M}_\lambda^{(1)}$  can then be written as

$$\begin{aligned} \mathcal{V}^{(2)} = & \frac{1}{N} \sum_{\lambda, \text{color}} 2\text{Re} \left( \mathcal{M}_\lambda^{*(1)} \mathcal{M}_{\lambda,A_h}^{(2)} \right. \\ & \left. + \mathcal{M}_\lambda^{*(1)} \left( \mathcal{M}_{\lambda,A_t}^{(2)} + \mathcal{M}_{\lambda,B}^{(2)} + \mathcal{M}_{\lambda,C}^{(2)} \right) \right). \end{aligned} \quad (5)$$

We sample the first interference term using massive virtual amplitude evaluations distributed according to unweighted events based on the top-quark only Born distribution, as described below. The remaining Born-virtual interference terms are evaluated with higher statistics: they are sampled dynamically by our phase-space generator code using the VEGAS algorithm [55,56], with an additional weight to ensure that sufficiently many events are generated at high invariant mass.

By default, we use the  $q_T$  subtraction scheme [57] for our two-loop amplitudes and the Catani-Seymour scheme [58] to construct the dipoles for our real radiation diagrams. This mismatch amounts to a term proportional to the Born contribution, which is straightforward to add (subtract) from the virtual (real) contributions as we desire. Similarly, we can obtain the virtual and real contributions in the original Catani subtraction scheme [59] by adding terms proportional to the Born contribution. Starting with the  $\mathbf{I}$  operator in the  $q_T$  scheme, we can obtain results in the Catani and Catani-Seymour subtraction schemes by adding  $2\text{Re}(\Delta\mathbf{I}) \cdot \mathcal{V}^{(1)}$  to  $\mathcal{V}^{(2)}$ , where

$$\Delta\mathbf{I}_C = -\frac{1}{2}\pi^2 C_A + i\pi\beta_0, \quad (6)$$

$$\Delta\mathbf{I}_{CS} = -i\pi C_A \left[ \frac{1}{\epsilon} + \ln\left(\frac{\mu_R^2}{\hat{s}}\right) \right] - \frac{\pi^2 C_A}{3} + \beta_0 + k_g, \quad (7)$$

with the Mandelstam invariant  $\hat{s} = (p_1 + p_2)^2$ ,  $\beta_0 = (11/6)C_A - (2/3)T_F n_f$  and  $k_g = (67/18 - \pi^2/6)C_A - (10/9)T_F n_f$ . The imaginary parts of the shifts do not contribute when computing the Born-virtual interference. We utilize these conversions to construct our virtual and real contributions in all three schemes ( $q_T$ , Catani-Seymour, and Catani).

The calculation of the class  $A_h$  massive virtual amplitudes was described in Ref. [31]. In the current work, the integrated virtual contribution is obtained using a new implementation of these amplitudes, relying on the distributed evaluation (DISTEVAL) feature of pySecDec, developed in tandem with this work. We evaluate 3000 unweighted events (distributed according to the Born cross section) on multiple GPUs. A major improvement, required to obtain sufficiently stable results in all phase-space

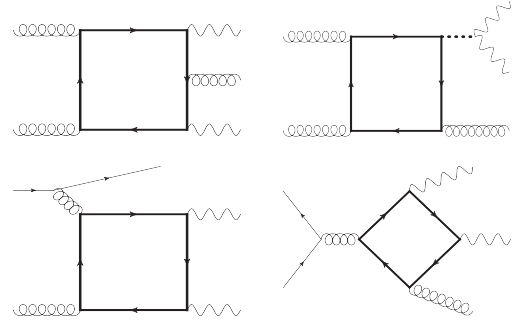


FIG. 2. Representative diagrams with a closed quark loop entering the real corrections to ZZ production. Different partonic channels and loops with light or top quarks contribute.

regions, is the evaluation of the two-loop amplitudes directly in the physical helicity basis (not the  $A$ -basis form factors presented in Refs. [20,31]), for which we set a relative accuracy target of 1% per amplitude. On a test grid of phase-space points, taken from Ref. [31], the mean evaluation time per phase-space point is 1.9 min with the new implementation and accuracy goal compared to 4.8 h with the original code. Our new virtual amplitude code is checked against our original code and an independent calculation using different methods described in Ref. [32].

Real contributions: The real corrections for this process include the partonic channels  $gg \rightarrow ZZ + g$ ,  $q(\bar{q})g \rightarrow ZZ + q(\bar{q})$ , and  $q\bar{q} \rightarrow ZZ + g$ ; representative Feynman diagrams are shown in Fig. 2. For the real radiation diagrams, we require that both  $Z$  bosons are coupled to the closed fermion loop; in particular, we exclude diagrams that involve a  $Z$  boson coupling to an incoming or outgoing quark line.

The amplitudes for the real radiation diagrams are generated using GoSam [60,61] and validated numerically at the level of individual phase-space points against MadGraph [62,63] and OpenLoops [64] (which uses COLLIER [65], CutTools [66], and OneLOop [67]). Our integrated real matrix elements are also validated against MadGraph by computing the LO ZZ plus jet cross section with several different values of  $p_{T,j}$  cut. To obtain stable numerical results we use the Ninja integrand reduction package [68,69] with a quadruple precision rescue system. Our rescue system employs a three-step procedure: each point is evaluated twice in double precision after an azimuthal rotation about the beam axis; if the double results do not agree to 11 digits, then the amplitude is reevaluated in quadruple precision; if the quadruple evaluation does not agree with the double results within eight digits, then a second rotated quadruple result is obtained. The result is discarded if the two quadruple results do not agree within 11 digits, affecting  $\sim 10^{-5}$  of the points. The most common feature of the rejected points is the presence of a soft jet. Soft and collinear singularities arising from the phase-space integration are cancelled locally by Catani-Seymour dipoles.

To obtain the Catani-Seymour dipole contributions, we compute the required spin-correlated Born matrix elements using the massless quark amplitudes from the `VVamp` library [20] and an in-house implementation of the one-loop massive quark amplitudes using `LoopTools` [70,71] to evaluate the one-loop master integrals. For the calculation of the dipoles, we observed that the spin-correlated Born matrix elements were numerically unstable in highly soft or collinear regions using the form factors of [31]. Switching to the orthogonal form factors defined in [28] improved numerical stability, and much better cancellation in the singular regions was observed.

**Results**—In this section, we present our NLO results for  $ZZ$  production in the gluon channel for the LHC. We set  $G_F = 1.1663787 \times 10^{-5} \text{ GeV}^{-2}$ ,  $m_Z = 91.1874 \text{ GeV}$ ,  $m_W = 80.2959 \text{ GeV}$ , and  $m_t = 173.016 \text{ GeV}$ . For the calculation of the two-loop massive amplitudes, we fix the ratio  $m_Z^2/m_t^2 = 5/18$  as described in [31]. We set  $\mu_R = \mu_f = m_{ZZ}/2$  as central values for renormalization and factorization scales respectively, and use the CT18NLO [72] parton distribution functions interfaced via LHAPDF [73] to calculate the total cross section. Uncertainty estimates are obtained by simultaneously varying the renormalization and factorization scales by a factor of 2 around the central scale  $\mu = m_{ZZ}/2$ .

In Fig. 3, we show the invariant mass distribution for this process considering only diagrams of class  $A_h$ , i.e., contributions involving both  $Z$  bosons coupled to the same closed top-quark loop. The shaded bands indicate the scale uncertainty. We find that the massive NLO corrections are large, enhancing the top-only cross section by a factor of 1.8 at  $\sqrt{s} = 13 \text{ TeV}$  hadronic center-of-mass energy. The NLO corrections to the  $Z$ -boson invariant mass distribution are large but rather flat; they amount to a factor 2 increase in the distribution near the  $ZZ$  production threshold and decrease to a factor of around 1.7 at 1 TeV. For the corresponding integrated cross section at  $\sqrt{s} = 13 \text{ TeV}$  we obtain,  $\sigma_{\text{LO}}^{A_h} = 19.00_{-21.4\%}^{+29.4\%} \text{ fb}$ ,  $\sigma_{\text{NLO}}^{A_h} = 34.46(6)_{-14.4\%}^{+16.4\%} \text{ fb}$ , where the number in parenthesis indicates the statistical Monte Carlo error.

In Fig. 3, we also show the subtracted virtual contribution obtained using different IR subtraction schemes. The NLO result does not depend on the choice of subtraction scheme, with different schemes amounting to reshuffling contributions proportional to  $\mathcal{V}^{(1)}$  between the subtracted reals and virtuals. However, we do observe that while the virtuals in the  $q_T$  and Catani-Seymour schemes behave rather similarly, they are heavily suppressed in the Catani scheme. The shape of the Catani scheme virtual corrections is similar to the other schemes, but the corrections are shifted down and are negative in the bins  $m_{ZZ} < 220 \text{ GeV}$  and  $m_{ZZ} > 620 \text{ GeV}$ . This implies that in the Catani scheme, the majority of the NLO correction comes from the IR subtracted real contribution and the subtracted virtual contribution accounts for less than 2% of the total

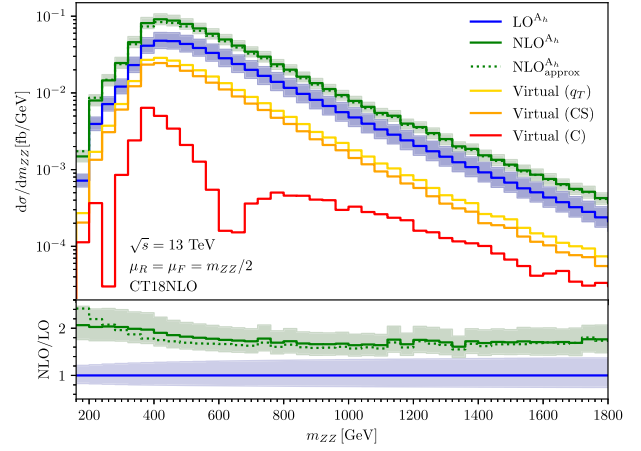


FIG. 3. Top-quark-only contributions to the  $ZZ$  invariant mass distribution in  $pp$  collisions. The absolute value of the two-loop virtual correction is shown separately in the  $q_T$ , Catani-Seymour (CS), and Catani (C) schemes. The dashed curve represents an approximate NLO result obtained by rescaling the massive Born amplitude with the massless K-factor.

cross section. We point out that the finite remainders in the Catani scheme were previously shown to be more sensitive to kinematic expansions of the two-loop expressions than in the  $q_T$  scheme [31], and may thus be interpreted as representing more directly the genuine two-loop effects. Choosing a scheme where the virtuals are numerically small can be of practical importance in situations where their exact evaluation is possible but computationally expensive, since one can reduce the number of phase-space points for the numerical integration in this way. Nevertheless, in the present work, we were able to obtain sufficient statistics that the virtuals could be reliably obtained in each subtraction scheme, as shown.

We also compare our results to an approximation,  $\text{NLO}_{\text{approx}}^{A_h}$  similar to [19], obtained using exact ingredients except for the massive two-loop virtual amplitudes, which are replaced by the top-quark only Born amplitude rescaled by the ratio  $\frac{1}{2}\mathcal{V}^{(2)}/\mathcal{V}^{(1)}$  computed using only the massless quark amplitudes. This rescaling is performed fully differentially at the level of individual phase-space points. We find that the approximation describes the exact results well in most of the phase space for the unpolarized distributions, particularly in the high energy region.

In other loop-induced processes, an uncertainty related to the choice of the top-quark mass renormalization scheme and scale is known to be large at NLO, dominating the QCD scale uncertainty [74–77]. To estimate this uncertainty, we can compare the result in the on-shell (OS) scheme with a result in the  $\overline{\text{MS}}$  scheme at the scale  $\mu_t = 2m_t^{\text{OS}}$ . Converting the top-quark mass to the  $\overline{\text{MS}}$  scheme we obtain  $m_t(\mu_t) = 154.6 \text{ GeV}$  [78,79]. Considering  $\sigma_{\text{LO}}^{A_h}$  only, at LO we find that the  $\overline{\text{MS}}$  result is 8.7% larger than the OS result.



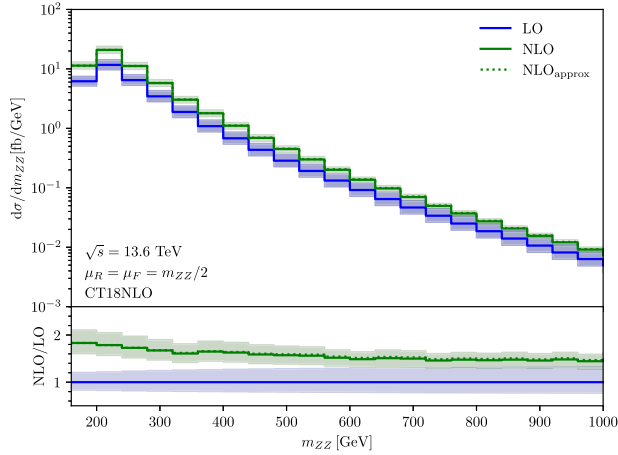


FIG. 4. Diboson invariant mass distribution for gluon-initiated  $ZZ$  production at the LHC. The solid curves represent the LO and NLO results with complete massless and massive contributions, including Higgs-mediated diagrams. The dashed curve represents an approximate NLO result obtained as described in the text.

In our calculation, the ratio of the mass of the  $Z$  boson and the top quark is fixed to the OS value in the two-loop virtual correction, preventing the direct evaluation of the scheme uncertainty at NLO. To estimate the size of the uncertainty, we can renormalize the top-quark mass in the  $\overline{\text{MS}}$  scheme and vary the mass in all parts of the calculation except the finite  $\mathcal{O}(\epsilon^0)$  term of the bare two-loop amplitude. We find that at NLO the  $\overline{\text{MS}}$  result is  $4.1 \pm 0.4\%$  bigger than the OS result. The stability of our estimate is assessed by computing it in both the Catani and  $q_T$  subtraction schemes.

In Fig. 4, we show the invariant mass distribution for  $ZZ$  production in the gluon channel for the LHC with  $\sqrt{s} = 13.6$  TeV, taking into account all massless and massive contributions, including those mediated by a Higgs boson. As above, the shaded bands indicate the scale uncertainty. We find that the complete NLO corrections are large, ranging from 1.8 near the  $ZZ$  production threshold and dropping to around 1.4 at 1 TeV invariant mass.

For the dashed curve,  $\text{NLO}_{\text{approx}}$ , we again employ the approximation in which the two-loop massive virtual amplitude is replaced by the rescaled top-quark only Born amplitude, as described above. At low invariant mass, the cross section is dominated by diagrams containing loops of massless quarks and, to a lesser extent, their interference with the Higgs-mediated contribution, both of which are included exactly in the approximation. Conversely, at high invariant mass, where the massive contribution is more important, the massive amplitudes are approximated well. As a result, we observe that the approximation works well across the entire invariant mass range for the full unpolarized NLO correction.

For the full NLO cross section in the gluon channel at  $\sqrt{s} = 13.6$  TeV with exact dependence on the top-quark mass, we obtain

$$\sigma_{\text{LO}} = 1316_{-18.0\%}^{+23.0\%} \text{ fb}, \quad (8)$$

$$\sigma_{\text{NLO}} = 2275(12)_{-12.0\%}^{+14.0\%} \text{ fb}. \quad (9)$$

Here, the number in parenthesis indicates the statistical Monte Carlo error, while the percentages specify the uncertainty stemming from simultaneous variation of the renormalization and factorization scales by a factor of 2. The complete NLO corrections to the gluon channel are large, increasing the contribution by a factor of 1.7 compared to the leading order and beyond the naive scale uncertainty estimate. The corrections approximately half the scale uncertainty. The impact of including the direct massive and Higgs-mediated contributions at the level of the total cross section is moderate, decreasing the NLO cross section by around 2% compared to purely massless contributions.

*Conclusions*—We have presented a complete calculation of the NLO QCD corrections to  $gg \rightarrow ZZ$  retaining full top-quark mass effects. For the LHC at center-of-mass energy  $\sqrt{s} = 13.6$  TeV, we find that the total cross section of the gluon-induced channel is enhanced by a factor of 1.7 relative to the LO correction. The diboson invariant mass distribution  $K$  factor falls from around 1.8 at production threshold to 1.4 at 1 TeV.

We show that the choice of infrared subtraction scheme has a great impact on the accuracy with which the two-loop finite remainders need to be known. In particular, we find that in Catani’s original subtraction scheme, the virtual contributions are numerically suppressed. This observation can help to reduce the computational cost for sampling these challenging contributions and should be taken into account when quantifying the quality of approximations for the finite remainders. Our analysis also shows that an approximation of the two-loop massive amplitudes similar to [19] works well at the level of the full unpolarized NLO invariant mass distribution.

In future work, it would be interesting to study the impact of top-quark mass effects on other differential observables and in the presence of anomalous couplings, e.g.,  $Zt\bar{t}$  [80,81]. We observe that at high invariant mass there is strong destructive interference at LO as well as NLO between diagrams in which the  $Z$  bosons couple directly to a massive quark line and those in which the  $Z$  bosons are produced via an intermediate Higgs boson; this cancellation could be spoiled by such anomalous couplings. The corrections presented here contribute at next-to-next-to-leading order to the hadronic cross section, and should be combined with the quark-initiated contributions at least to NNLO for such phenomenological applications.

*Acknowledgments*—We would like to thank Gudrun Heinrich, Stephan Jahn, and C.-P. Yuan for useful discussions and related work. This research was supported by the Deutsche Forschungsgemeinschaft (DFG, German Research Foundation) through Grant 396021762—TRR 257, the National Science Foundation through Grant 2013859, the Royal Society through the University Research Fellowship Grant URF/R1/201268, and the UK Science and Technology Facilities Council through Grant ST/X000745/1. We gratefully acknowledge support and resources provided by the High Performance Computing Center (HPCC) at Michigan State University. Our Feynman diagrams were generated using JaxoDraw [82], based on AxoDraw [83].

- 
- [1] G. Aad *et al.* (ATLAS Collaboration), Search for heavy resonances decaying into a pair of Z bosons in the  $\ell^+\ell^-\ell^+\ell^-$  and  $\ell^+\ell^-\nu\bar{\nu}$  final states using  $139\text{ fb}^{-1}$  of proton–proton collisions at  $\sqrt{s} = 13\text{ TeV}$  with the ATLAS detector, *Eur. Phys. J. C* **81**, 332 (2021).
- [2] G. Aad *et al.* (ATLAS Collaboration), Search for heavy diboson resonances in semileptonic final states in pp collisions at  $\sqrt{s} = 13\text{ TeV}$  with the ATLAS detector, *Eur. Phys. J. C* **80**, 1165 (2020).
- [3] A. Tumasyan *et al.* (CMS Collaboration), Search for heavy resonances decaying to  $Z(\nu\bar{\nu})V(q\bar{q}')$  in proton-proton collisions at  $\sqrt{s} = 13\text{ TeV}$ , *Phys. Rev. D* **106**, 012004 (2022).
- [4] A. M. Sirunyan *et al.* (CMS Collaboration), A multi-dimensional search for new heavy resonances decaying to boosted WW, WZ, or ZZ boson pairs in the dijet final state at 13 TeV, *Eur. Phys. J. C* **80**, 237 (2020).
- [5] M. Aaboud *et al.* (ATLAS Collaboration), Constraints on off-shell Higgs boson production and the Higgs boson total width in  $ZZ \rightarrow 4\ell$  and  $ZZ \rightarrow 2\ell 2\nu$  final states with the ATLAS detector, *Phys. Lett. B* **786**, 223 (2018).
- [6] A. M. Sirunyan *et al.* (CMS Collaboration), Measurement and interpretation of differential cross sections for Higgs boson production at  $\sqrt{s} = 13\text{ TeV}$ , *Phys. Lett. B* **792**, 369 (2019).
- [7] A. M. Sirunyan *et al.* (CMS Collaboration), Measurements of the Higgs boson width and anomalous  $HVV$  couplings from on-shell and off-shell production in the four-lepton final state, *Phys. Rev. D* **99**, 112003 (2019).
- [8] G. Aad *et al.* (ATLAS Collaboration), Measurements of the Higgs boson inclusive and differential fiducial cross sections in the  $4\ell$  decay channel at  $\sqrt{s} = 13\text{ TeV}$ , *Eur. Phys. J. C* **80**, 942 (2020).
- [9] G. Aad *et al.* (ATLAS Collaboration), Measurement of ZZ production cross-sections in the four-lepton final state in pp collisions at  $\sqrt{s} = 13.6\text{ TeV}$  with the ATLAS experiment, *Phys. Lett. B* **855**, 138764 (2024).
- [10] G. Aad *et al.* (ATLAS Collaboration), Evidence of pair production of longitudinally polarised vector bosons and study of CP properties in  $ZZ \rightarrow 4\ell$  events with the ATLAS detector at  $\sqrt{s} = 13\text{ TeV}$ , *J. High Energy Phys.* **12** (2023) 107.
- [11] F. Caola and K. Melnikov, Constraining the Higgs boson width with ZZ production at the LHC, *Phys. Rev. D* **88**, 054024 (2013).
- [12] J. M. Campbell, R. K. Ellis, and C. Williams, Bounding the Higgs width at the LHC using full analytic results for  $gg \rightarrow e^-e^+\mu^-\mu^+$ , *J. High Energy Phys.* **04** (2014) 060.
- [13] N. Kauer and G. Passarino, Inadequacy of zero-width approximation for a light Higgs boson signal, *J. High Energy Phys.* **08** (2012) 116.
- [14] N. Kauer, Interference effects for  $H \rightarrow WW/ZZ \rightarrow \ell\bar{\nu}_\ell\bar{\ell}\nu_\ell$  searches in gluon fusion at the LHC, *J. High Energy Phys.* **12** (2013) 082.
- [15] A. Tumasyan *et al.* (CMS Collaboration), Measurement of the Higgs boson width and evidence of its off-shell contributions to ZZ production, *Nat. Phys.* **18**, 1329 (2022).
- [16] G. Aad *et al.* (ATLAS Collaboration), Evidence of off-shell Higgs boson production from ZZ leptonic decay channels and constraints on its total width with the ATLAS detector, *Phys. Lett. B* **846**, 138223 (2023).
- [17] F. Cascioli, T. Gehrmann, M. Grazzini, S. Kallweit, P. Maierhöfer, A. von Manteuffel, S. Pozzorini, D. Rathlev, L. Tancredi, and E. Weihs, ZZ production at hadron colliders in NNLO QCD, *Phys. Lett. B* **735**, 311 (2014).
- [18] F. Caola, K. Melnikov, R. Rötsch, and L. Tancredi, QCD corrections to ZZ production in gluon fusion at the LHC, *Phys. Rev. D* **92**, 094028 (2015).
- [19] M. Grazzini, S. Kallweit, M. Wiesemann, and J. Y. Yook, ZZ production at the LHC: NLO QCD corrections to the loop-induced gluon fusion channel, *J. High Energy Phys.* **03** (2019) 070.
- [20] A. von Manteuffel and L. Tancredi, The two-loop helicity amplitudes for  $gg \rightarrow V_1V_2 \rightarrow 4\text{ leptons}$ , *J. High Energy Phys.* **06** (2015) 197.
- [21] F. Caola, J. M. Henn, K. Melnikov, A. V. Smirnov, and V. A. Smirnov, Two-loop helicity amplitudes for the production of two off-shell electroweak bosons in gluon fusion, *J. High Energy Phys.* **06** (2015) 129.
- [22] B. W. Lee, C. Quigg, and H. B. Thacker, Weak interactions at very high-energies: The role of the Higgs boson mass, *Phys. Rev. D* **16**, 1519 (1977).
- [23] M. S. Chanowitz and M. K. Gaillard, The TeV physics of strongly interacting W's and Z's, *Nucl. Phys.* **B261**, 379 (1985).
- [24] K. Melnikov and M. Dowling, Production of two Z-bosons in gluon fusion in the heavy top quark approximation, *Phys. Lett. B* **744**, 43 (2015).
- [25] F. Caola, M. Dowling, K. Melnikov, R. Rötsch, and L. Tancredi, QCD corrections to vector boson pair production in gluon fusion including interference effects with off-shell Higgs at the LHC, *J. High Energy Phys.* **07** (2016) 087.
- [26] J. M. Campbell, R. K. Ellis, M. Czakon, and S. Kirchner, Two loop correction to interference in  $gg \rightarrow ZZ$ , *J. High Energy Phys.* **08** (2016) 011.
- [27] R. Gröber, A. Maier, and T. Rauh, Top quark mass effects in  $gg \rightarrow ZZ$  at two loops and off-shell Higgs interference, *Phys. Rev. D* **100**, 114013 (2019).
- [28] J. Davies, G. Mishima, M. Steinhauser, and D. Wellmann,  $gg \rightarrow ZZ$ : Analytic two-loop results for the low- and high-energy regions, *J. High Energy Phys.* **04** (2020) 024.

- [29] S. Alioli, S. Ferrario Ravasio, J. M. Lindert, and R. Rötsch, Four-lepton production in gluon fusion at NLO matched to parton showers, *Eur. Phys. J. C* **81**, 687 (2021).
- [30] L. Buonocore, G. Koole, D. Lombardi, L. Rottoli, M. Wiesemann, and G. Zanderighi, ZZ production at nNNLO + PS with MiNNLO<sub>PS</sub>, *J. High Energy Phys.* **01** (2022) 072.
- [31] B. Agarwal, S. P. Jones, and A. von Manteuffel, Two-loop helicity amplitudes for  $gg \rightarrow ZZ$  with full top-quark mass effects, *J. High Energy Phys.* **05** (2021) 256.
- [32] C. Brønnum-Hansen and C.-Y. Wang, Top quark contribution to two-loop helicity amplitudes for Z boson pair production in gluon fusion, *J. High Energy Phys.* **05** (2021) 244.
- [33] D. A. Dicus, C. Kao, and W. W. Repko, Gluon production of gauge bosons, *Phys. Rev. D* **36**, 1570 (1987).
- [34] E. W. N. Glover and J. J. van der Bij, Z boson pair production via gluon fusion, *Nucl. Phys.* **B321**, 561 (1989).
- [35] C. Zecher, T. Matsuura, and J. van der Bij, Leptonic signals from off-shell Z boson pairs at hadron colliders, *Z. Phys. C* **64**, 219 (1994).
- [36] J. Gluza, K. Kajda, and D. A. Kosower, Towards a basis for planar two-loop integrals, *Phys. Rev. D* **83**, 045012 (2011).
- [37] R. M. Schabinger, A new algorithm for the generation of unitarity-compatible integration by parts relations, *J. High Energy Phys.* **01** (2012) 077.
- [38] H. Ita, Two-loop integrand decomposition into master integrals and surface terms, *Phys. Rev. D* **94**, 116015 (2016).
- [39] K. J. Larsen and Y. Zhang, Integration-by-parts reductions from unitarity cuts and algebraic geometry, *Phys. Rev. D* **93**, 041701(R) (2016).
- [40] J. Böhm, A. Georgoudis, K. J. Larsen, M. Schulze, and Y. Zhang, Complete sets of logarithmic vector fields for integration-by-parts identities of Feynman integrals, *Phys. Rev. D* **98**, 025023 (2018).
- [41] A. von Manteuffel and R. M. Schabinger, A novel approach to integration by parts reduction, *Phys. Lett. B* **744**, 101 (2015).
- [42] T. Peraro, Scattering amplitudes over finite fields and multivariate functional reconstruction, *J. High Energy Phys.* **12** (2016) 030.
- [43] S. Abreu, J. Dormans, F. Febres Cordero, H. Ita, B. Page, and V. Sotnikov, Analytic form of the planar two-loop five-parton scattering amplitudes in QCD, *J. High Energy Phys.* **05** (2019) 084.
- [44] J. Boehm, M. Wittmann, Z. Wu, Y. Xu, and Y. Zhang, IBP reduction coefficients made simple, *J. High Energy Phys.* **12** (2020) 054.
- [45] H. A. Chawdhry, M. Czakon, A. Mitov, and R. Poncelet, Two-loop leading-color helicity amplitudes for three-photon production at the LHC, *J. High Energy Phys.* **06** (2021) 150.
- [46] M. Heller and A. von Manteuffel, MultivariateApart: Generalized partial fractions, *Comput. Phys. Commun.* **271**, 108174 (2022).
- [47] B. Agarwal, F. Buccioni, A. von Manteuffel, and L. Tancredi, Two-loop leading colour QCD corrections to  $q\bar{q} \rightarrow \gamma\gamma g$  and  $qg \rightarrow \gamma\gamma q$ , *J. High Energy Phys.* **04** (2021) 201.
- [48] S. Borowka, G. Heinrich, S. Jahn, S. Jones, M. Kerner, and J. Schlenk, A GPU compatible quasi-Monte Carlo integrator interfaced to pySecDec, *Comput. Phys. Commun.* **240**, 120 (2019).
- [49] G. Heinrich, S. Jahn, S. P. Jones, M. Kerner, F. Langer, V. Magerya, A. Pöldaru, J. Schlenk, and E. Villa, Expansion by regions with pySecDec, *Comput. Phys. Commun.* **273**, 108267 (2022).
- [50] G. Heinrich, S. P. Jones, M. Kerner, V. Magerya, A. Olsson, and J. Schlenk, Numerical scattering amplitudes with pySecDec, *Comput. Phys. Commun.* **295**, 108956 (2024).
- [51] T. Gehrmann, A. von Manteuffel, and L. Tancredi, The two-loop helicity amplitudes for  $q\bar{q}' \rightarrow V_1 V_2 \rightarrow 4$  leptons, *J. High Energy Phys.* **09** (2015) 128.
- [52] J. Vollinga and S. Weinzierl, Numerical evaluation of multiple polylogarithms, *Comput. Phys. Commun.* **167**, 177 (2005).
- [53] C. W. Bauer, A. Frink, and R. Kreckel, Introduction to the GiNaC framework for symbolic computation within the C++ programming language, *J. Symb. Comput.* **33**, 1 (2002).
- [54] C. Anastasiou, S. Beerli, S. Bucherer, A. Daleo, and Z. Kunszt, Two-loop amplitudes and master integrals for the production of a Higgs boson via a massive quark and a scalar-quark loop, *J. High Energy Phys.* **01** (2007) 082.
- [55] G. P. Lepage, A new algorithm for adaptive multidimensional integration, *J. Comput. Phys.* **27**, 192 (1978).
- [56] T. Hahn, CUBA: A Library for multidimensional numerical integration, *Comput. Phys. Commun.* **168**, 78 (2005).
- [57] S. Catani, L. Cieri, D. de Florian, G. Ferrera, and M. Grazzini, Universality of transverse-momentum resummation and hard factors at the NNLO, *Nucl. Phys.* **B881**, 414 (2014).
- [58] S. Catani and M. H. Seymour, A general algorithm for calculating jet cross-sections in NLO QCD, *Nucl. Phys.* **B485**, 291 (1997); **B510**, 503(E) (1998).
- [59] S. Catani, The singular behavior of QCD amplitudes at two loop order, *Phys. Lett. B* **427**, 161 (1998).
- [60] G. Cullen, N. Greiner, G. Heinrich, G. Luisoni, P. Mastrolia, G. Ossola, T. Reiter, and F. Tramontano (GoSam Collaboration), Automated one-loop calculations with GoSam, *Eur. Phys. J. C* **72**, 1889 (2012).
- [61] G. Cullen *et al.* (GoSam Collaboration), GOSAM-2.0: A tool for automated one-loop calculations within the standard model and beyond, *Eur. Phys. J. C* **74**, 3001 (2014).
- [62] J. Alwall, R. Frederix, S. Frixione, V. Hirschi, F. Maltoni, O. Mattelaer, H. S. Shao, T. Stelzer, P. Torrielli, and M. Zaro, The automated computation of tree-level and next-to-leading order differential cross sections, and their matching to parton shower simulations, *J. High Energy Phys.* **07** (2014) 079.
- [63] R. Frederix, S. Frixione, V. Hirschi, D. Pagani, H. S. Shao, and M. Zaro, The automation of next-to-leading order electroweak calculations, *J. High Energy Phys.* **07** (2018) 185; **11** (2021) 85.
- [64] F. Buccioni, J.-N. Lang, J. M. Lindert, P. Maierhöfer, S. Pozzorini, H. Zhang, and M. F. Zoller, OpenLoops 2, *Eur. Phys. J. C* **79**, 866 (2019).
- [65] A. Denner, S. Dittmaier, and L. Hofer, Collier: A fortran-based complex one-loop Library in extended regularizations, *Comput. Phys. Commun.* **212**, 220 (2017).
- [66] G. Ossola, C. G. Papadopoulos, and R. Pittau, CutTools: A program implementing the OPP reduction method to

- compute one-loop amplitudes, *J. High Energy Phys.* **03** (2008) 042.
- [67] A. van Hameren, OneLoop: For the evaluation of one-loop scalar functions, *Comput. Phys. Commun.* **182**, 2427 (2011).
- [68] P. Mastrolia, E. Mirabella, and T. Peraro, Integrand reduction of one-loop scattering amplitudes through Laurent series expansion, *J. High Energy Phys.* **06** (2012) 095.
- [69] T. Peraro, Ninja: Automated integrand reduction via laurent expansion for one-loop amplitudes, *Comput. Phys. Commun.* **185**, 2771 (2014).
- [70] G. J. van Oldenborgh and J. A. M. Vermaseren, New algorithms for one loop integrals, *Z. Phys. C* **46**, 425 (1990).
- [71] T. Hahn and M. Perez-Victoria, Automatized one loop calculations in four-dimensions and D-dimensions, *Comput. Phys. Commun.* **118**, 153 (1999).
- [72] T.-J. Hou *et al.*, New CTEQ global analysis of quantum chromodynamics with high-precision data from the LHC, *Phys. Rev. D* **103**, 014013 (2021).
- [73] A. Buckley, J. Ferrando, S. Lloyd, K. Nordström, B. Page, M. Rüfenacht, M. Schönherr, and G. Watt, LHAPDF6: Parton density access in the LHC precision era, *Eur. Phys. J. C* **75**, 132 (2015).
- [74] J. Baglio, F. Campanario, S. Glaus, M. Mühlleitner, M. Spira, and J. Streicher, Gluon fusion into Higgs pairs at NLO QCD and the top mass scheme, *Eur. Phys. J. C* **79**, 459 (2019).
- [75] J. Baglio, F. Campanario, S. Glaus, M. Mühlleitner, J. Ronca, and M. Spira,  $gg \rightarrow HH$ : Combined uncertainties, *Phys. Rev. D* **103**, 056002 (2021).
- [76] L. Chen, J. Davies, G. Heinrich, S. P. Jones, M. Kerner, G. Mishima, J. Schlenk, and M. Steinhauser, ZH production in gluon fusion at NLO in QCD, *J. High Energy Phys.* **08** (2022) 056.
- [77] G. Degrossi, R. Gröber, M. Vitti, and X. Zhao, On the NLO QCD corrections to gluon-initiated ZH production, *J. High Energy Phys.* **08** (2022) 009.
- [78] K. G. Chetyrkin, J. H. Kuhn, and M. Steinhauser, RunDec: A Mathematica package for running and decoupling of the strong coupling and quark masses, *Comput. Phys. Commun.* **133**, 43 (2000).
- [79] F. Herren and M. Steinhauser, Version 3 of RunDec and CRunDec, *Comput. Phys. Commun.* **224**, 333 (2018).
- [80] A. Azatov, C. Grojean, A. Paul, and E. Salvioni, Resolving gluon fusion loops at current and future hadron colliders, *J. High Energy Phys.* **09** (2016) 123.
- [81] Q.-H. Cao, B. Yan, C. P. Yuan, and Y. Zhang, Probing  $Z\bar{t}t$  couplings using  $Z$  boson polarization in  $ZZ$  production at hadron colliders, *Phys. Rev. D* **102**, 055010 (2020).
- [82] D. Binosi and L. Theussl, JaxoDraw: A graphical user interface for drawing Feynman diagrams, *Comput. Phys. Commun.* **161**, 76 (2004).
- [83] J. A. M. Vermaseren, AxoDraw, *Comput. Phys. Commun.* **83**, 45 (1994).